Revealing Water Structure at Neutral and Charged Graphene/Water Interfaces through Quantum Simulations of Sum Frequency Generation Spectra

Richa Rashmi,[†,⊥] Toheeb O Balogun,[‡,⊥] Golam Azom,[‡] Henry Agnew,[†] Revati Kumar,[*,‡] and Francesco Paesani[*,†,¶,§,‖]

†*Department of Chemistry and Biochemistry, University of California San Diego, La Jolla, California 92093, United States*

‡*Department of Chemistry, Louisiana State University, Baton Rouge, Louisiana 70803, United States*

¶*Materials Science and Engineering, University of California San Diego, La Jolla, California 92093, United States*

§*Halıcıoğlu Data Science Institute, University of California San Diego, La Jolla, California 92093, United States*

‖*San Diego Supercomputer Center, University of California San Diego, La Jolla, California 92093, United States*

⊥*Contributed equally to this work*

E-mail: revatik@lsu.edu; fpaesani@ucsd.edu

Abstract

The structure and dynamics of water at charged graphene interfaces fundamentally influence molecular responses to electric fields, with implications for applications in energy storage, catalysis, and surface chemistry. Leveraging the realism of the MB-pol data-driven many-body potential and advanced path-integral quantum dynamics, we analyze the vibrational sum-frequency generation (vSFG) spectrum of graphene/water interfaces under varying surface charges. Our quantum simulations reveal a distinctive dangling OH peak in the vSFG spectrum at neutral graphene, consistent with recent experimental findings yet markedly different from earlier studies. As the graphene surface becomes positively charged, interfacial water molecules reorient, decreasing the intensity of the dangling OH peak as the OH groups turn away from the graphene. In contrast, water molecules orient their OH bonds toward negatively charged graphene, leading to a prominent dangling OH peak in the corresponding vSFG spectrum. This charge-induced reorganization generates a diverse range of hydrogen-bonding topologies at the interface, driven by variations in the underlying electrostatic interactions. Remarkably, these structural changes extend into deeper water layers, creating an unequal distribution of molecules with OH bonds pointing toward and away from the graphene sheet. This imbalance amplifies bulk spectral features, underscoring the complexity of many-body interactions that shape the molecular structure of water at charged graphene interfaces.

Keywords

graphene, water, solid/liquid interfaces, hydrogen bonding, sum-frequency generation spectroscopy

Introduction

The physical and chemical properties of liquid water are largely driven by its dynamic network of hydrogen bonds.[1,2] Water molecules at interfaces exhibit distinct properties compared to those in bulk due to the disruption of the hydrogen-bond network by the phase boundary.[3] At the air/water interface, the interfacial depth is relatively shallow, effectively encompassing just one water layer.[4–6] In contrast, at electrode interfaces, the surface charge plays a dominant role in shaping the local hydrogen-bonding environment of water and the interfacial effects can extend well beyond the first molecular layer.[3] While the linear response approximation traditionally assumes that induced polarization is directly proportional to an applied electric field, interfacial water often exhibits significant nonlinear behavior.[7–10] Understanding these deviations from linearity requires careful study of molecular organization at interfaces, especially as charges on electrodes evolve with applied voltages, influencing the behavior of interfacial water under electric fields.

Graphene, a two-dimensional sheet of sp^2 hybridized carbon atoms arranged in a hexagonal lattice, provides an ideal platform for investigating such interfacial phenomena.[11] Graphene's exceptional chemical stability, mechanical flexibility, and outstanding electrical and thermal conductivity have positioned it as a key material for diverse applications, from water desalination and energy storage to chemosensing and electrocatalysis.[12–14] Understanding how graphene interacts with water is fundamental for improving wettability, friction, and local transport properties, which are, for example, key factors in advancing membrane design.[15] This significance has prompted numerous experimental and computational studies exploring the behavior of water at the graphene/water interface.[16]

Graphene's hydrophobicity and wettability are highly influenced by the properties of its underlying substrate. Although macroscopic wettability is typically assessed through water contact angle measurements, results can range from hydrophilic to hydrophobic due to airborne hydrocarbon contamination and variations in graphene's doping levels.[17–19] Graphene's near-transparency to infrared and visible light makes it well suited for surface-specific vibra-

tional sum-frequency generation (vSFG) spectroscopy, particularly in its heterodyne-detected implementation (HD-vSFG),[20] enabling direct insights into the molecular properties of the graphene/water interface.

The presence of dangling OH groups in vSFG spectra of water serves as a key indicator of structural reorganization at aqueous interfaces. In 2017, Singla *et al.* found no evidence of dangling OH stretch above 3500 cm^{-1} in the vSFG spectrum of the sapphire-supported graphene/water interface.[21] This observation was further supported by subsequent studies of single-sheet graphene on CaF_2 and SiO_2 substrates, where the vSFG signal was dominated by substrate effects, with interfacial water molecules trapped between the graphene and hydrophilic substrate complicating spectral interpretation.[22,23] In 2021, Montenegro *et al.* observed an asymmetric response and a sudden rearrangement of water molecules at the graphene/heavy water interface under an external electric field.[9] At potentials below -1.6 V, the vSFG spectrum of heavy water showed a dangling OD stretch, but this peak disappeared above -1.0 V. The study suggested that as the surface charge becomes positive, the dangling OD species rotate away from the graphene and form hydrogen bonds with water molecules in the underlying layer. Collectively, these findings suggested that neutral single-sheet graphene is not hydrophobic at the molecular level. Notably, vSFG experiments on multilayer graphene films demonstrated that hydrophobicity increases with film thickness, revealing a characteristic dangling OH peak around 3600 cm^{-1} when the number of graphene layers exceeds three.[24] In contrast, Yang *et al.* in a separate vSFG experiment of the graphene/electrolyte interface suggested that graphene exhibits hydrophobic behavior at zero or positive bias, and hydrophilic behavior at negative bias.[25] Recent HD-VSFG experiments by Wang *et al.* have emphasized the critical role of substrate effects,[26–28] proposing that the dangling OD peak observed in Ref. 9 at negative potential likely originated from substrate-trapped water molecules. However, the latest vSFG experiments on suspended graphene have indicated that neutral graphene is indeed hydrophobic,[29] highlighting how experimental conditions can significantly influence observed wettability.

Several molecular dynamics (MD) simulations have provided insights into the properties of the graphene/water interface and the corresponding experimental vSFG spectra. Rana et al. used ab initio molecular dynamics (AIMD) simulations with the BLYP functional to investigate graphene's hydrophobicity, revealing slower dynamics in interfacial water compared to bulk water molecules.[30] Ohto et al. performed AIMD simulations of the D_2O/graphene interface using the BLYP functional, predicting a dangling OD feature around 2645 cm^{-1} at zero applied field.[31] More recently, Wang et al. simulated the HD-vSFG spectrum of the suspended graphene/water interface with the revPBE+D3 functional. The study found that graphene weakly affects the dangling OH group, lowering its frequency through interaction with the graphene sheet, with minimal impact on hydrogen-bonded OH groups.[29] However, it has become evident that water models derived from density functional theory (DFT)[32] suffer from functional- and density-driven errors[33,34] that prevent them from accurately representing many-body interactions.[35] These inherent errors limits the reliability of DFT models, especially those derived within the generalized gradient approximation (GGA), in predicting structural[36] and thermodynamic properties[37,38] as well as vibrational spectra[39] of water across various phases and in different environments, particularly when nuclear quantum effects (NQEs) are properly accounted for in the simulations.[40]

Complementary computational studies have also been conducted using empirical water models. Joutsuka et al. applied the charge response kernel model to calculate the vSFG spectra of the water/air interface under varying electric fields, demonstrating that the intensity of the dangling OH peak increases with increasingly negative applied fields.[41] In a subsequent study, Zhang et al. used the SPC/E water model to study the graphene/water interface under a range of applied voltages, predicting a free OH peak at zero voltage and reporting increased intensity for the band corresponding to hydrogen-bonded OH groups with increasing voltage, which highlighted the importance of surface versus bulk contributions to the SFG signal.[42,43] Despite their success in reproducing some properties of water,[44] empirical models, however, fall short at providing a reliable representation of water across

all of its phases,[37] often requiring *ad hoc* temperature and/or pressure shifts to be effectively compared with experimental measurements. These limitations are particularly acute for modeling vibrational spectra of water at different thermodynamic states as the spectra not only depend on the underlying molecular configurations but also on the associated molecular dipole moments and polarizabilities, which are usually not accurately represented by empirical models.[45]

Most experimental vSFG studies on substrate-supported graphene have shown that the SFG signals are dominated by substrate effects, which preclude an unambiguous characterization of the properties of the graphene/water interface. On the other hand, previous theoretical studies have relied on empirical or DFT-based models that are known to be limited in their capability to accurately predict the properties of water. Furthermore, all previous studies have neglected the role of NQEs in influencing both the structure and vSFG spectra of water at charged graphene interfaces. To address these limitations and provide a realistic description of neutral and charged graphene/water interfaces, we performed systematic MD simulations using the MB-pol data-driven many-body potential of water,[46–49] which accurately predicts the properties of water across all molecular phases,[50,51] in combination with the temperature-elevated path integral coarse-graining (Te-PIGS) method,[52,53] which effectively accounts for NQEs. By systematically dissecting the spectral features of the simulated quantum HD-vSFG spectra in terms of distinct hydrogen-bonding topologies and molecular orientations, we provide a detailed molecular-level picture of the graphene/water interface as a function of graphene charge.

Results and Discussion

Structure of the graphene/water interface. Figure 1 shows a snapshot of the simulated graphene/water interface system, along with several properties calculated across the water slab from MD simulations conducted at 298 K. In the MD simulations carbon atoms

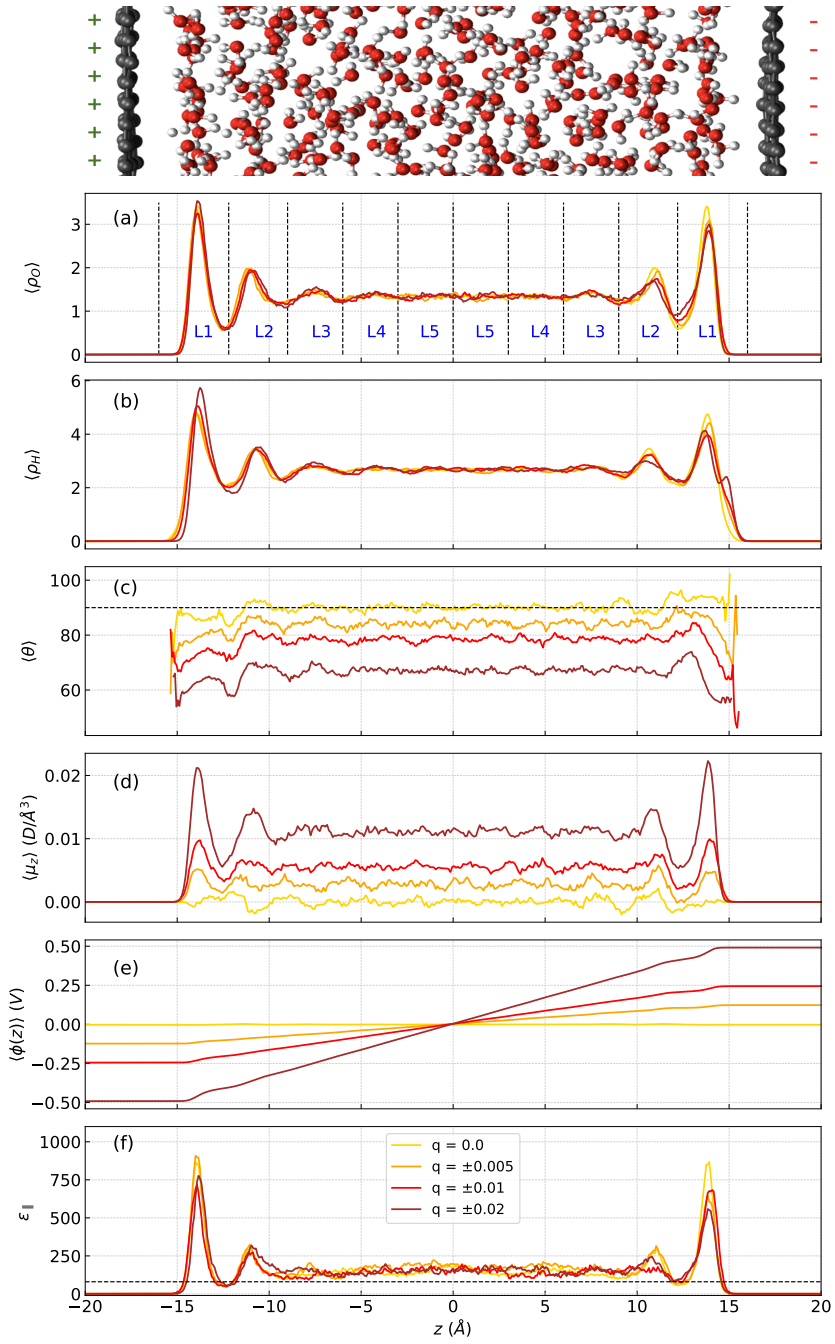

Figure 1: Snapshot of the simulated graphene/water interface system (top) along with several properties calculated across the water slab as a function of graphene charge ($q = 0.0e$, $q = \pm 0.005e$, $q = \pm 0.01e$, $q = \pm 0.02e$): (a) oxygen density profiles, (b) hydrogen density profiles, (c) average molecular orientations with respect to the surface normal of the negative graphene sheet, (d) induced dipole moment distributions, (e) electrostatic potentials, and (f) parallel dielectric profiles.

on opposing graphene sheets carry equal but opposite charges ($q = \pm\ 0.0e$, $\pm\ 0.005e$, $\pm\ 0.01e$, $\pm\ 0.02e$, where e is the elementary charge, corresponding to surface charges of $\pm\ 0.0, \pm\ 0.0289, \pm\ 0.0578$, and $\pm\ 0.115$ C/m^2, respectively). Hereafter, q defines the charge on each carbon atom of the graphene sheets. The oxygen density profiles (Figure 1a) indicate the presence of approximately three distinct hydration layers near each of the graphene sheets, with the third layer becoming more pronounced at higher charges. These variations are more prominent at the negatively charged graphene sheet, where increasing negative charge leads to less ordered water layers. The hydrogen density profiles (Figure 1b) reveal a distinct peak at $q = -0.02e$, indicating that some water molecules move closer to the interface, with their OH bonds pointing toward it. Figure 1c shows the average angular orientation of water molecules relative to the surface normal of the negatively charged graphene sheet. The average angular orientation of water molecules at the neutral graphene/water interface is similar to that observed at the air/water interface. At higher q values, water molecules increasingly orient toward the negatively charged graphene sheet under the influence of the effective electric field generated between the oppositely charged interfaces. This effect is also evident from the average induced dipole moment of water molecules along the z-axis (Figure 1d), where the dipole moment is zero only for neutral graphene and grows as the graphene charge density increases. The electrostatic potential in the water slab along the z-axis (Figure 1e) shows that the slope of the potential increases with increasing surface charge values and becomes constant beyond a few molecular layers from the graphene sheets. In contrast, the parallel dielectric profile along the z-axis (Figure 1f) is found to be higher than bulk water but remains unchanged across different surface charge values. Moreover, the tetrahedral order parameter of water molecules in the L1 layer (Figure 1a) shows some variation with different graphene surface charges, but remains unchanged in deeper layers (see Figure S1 in Supplementary Information). Figure S11 shows results from a similar analysis conducted for a larger system demonstrating that these orientational changes are not a result of finite size effects.

Orientational analysis. To further elucidate the structural arrangements of interfacial water molecules, we analyzed their orientations in response to varying surface charge values on the two graphene sheets. Figure 2 shows the joint probability density distribution $\mathcal{P}(\cos\theta_{\mathrm{DW}}, \cos\theta_{\mathrm{HH}})$ for water molecules[54–57] in the L1 layer (Figure 1) for $q = -0.02e$, $q = 0.0e$, and $q = +0.02e$. In this analysis, θ_{HH} represents the angle between the vector $\mathbf{V}_{\mathrm{HH}}$ connecting the two hydrogen atoms of a water molecule (pointing from the hydrogen atom further from the surface to the hydrogen atom closer to the surface), and the vector normal to the instantaneous water surface, $\mathbf{V}_{\mathrm{S}}$, as shown in Figure 2a. Similarly, θ_{DW} represents the angle between the water dipole vector, $\mathbf{V}_{\mathrm{W}}$, and $\mathbf{V}_{\mathrm{S}}$, as shown in Figure 2b. Six primary regions (Figure 2i) are identified within the $(\cos\theta_{\mathrm{DW}}, \cos\theta_{\mathrm{HH}})$ distribution, each corresponding to distinct molecular orientations: (i) BT: both OH bonds pointing toward the graphene sheet (Figure 2c), (ii) VT: vertical OH bond pointing toward the graphene sheet (dangling

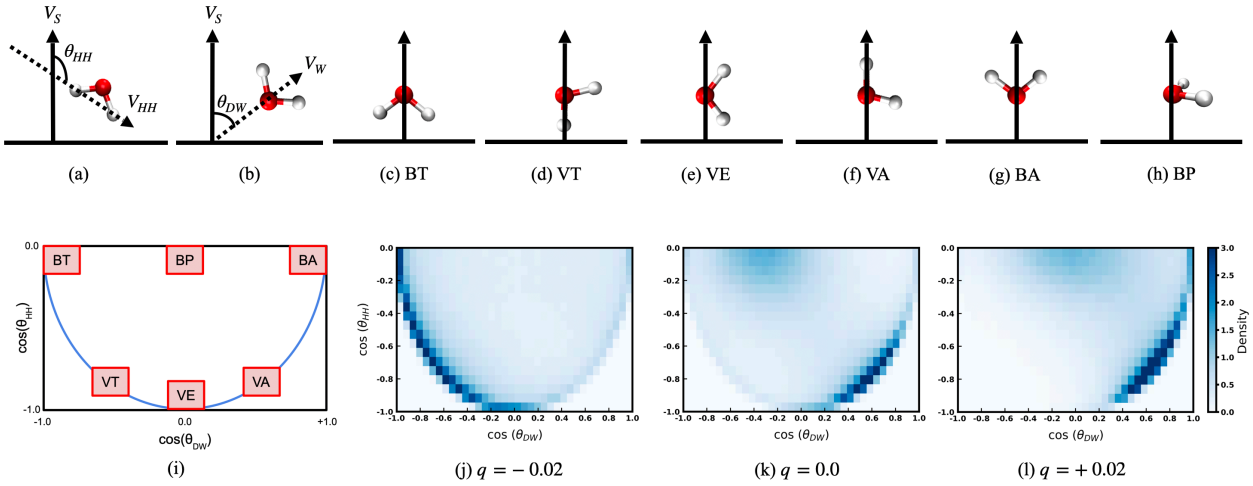

Figure 2: Schematic representation of the angles θ_{HH} (a) and θ_{DW} (b) used in the analysis of water orientations at the interface with a graphene sheet. Representative configurations of a water molecule at the interface with a graphene sheet: (c) both OH bonds toward the graphene sheet (BT); (d) vertical OH bond toward the graphene sheet (VT); (e) both OH bonds vertical to the graphene sheet (VE); (f) vertical OH bond away from the graphene sheet (VA); (g) both OH bonds away from the graphene sheet (BA); and (h) both OH bonds parallel to the graphene sheet (BP). Joint probability density distribution $\mathcal{P}(\cos\theta_{\mathrm{DW}}, \cos\theta_{\mathrm{HH}})$ for water molecules in the L1 layer at different graphene charges: (j) $q = -0.02e$, (k) $q = 0.0e$, and (l) $q = +0.02e$. Panel (i) shows the ideal regions of the various molecular configurations on the joint probability density distribution map.

OH) (Figure 2d), (iii) VE: both OH bonds oriented vertically relative to the graphene sheet (Figure 2e), (iv) VA: vertical OH bond pointing away from the graphene sheet (Figure 2f), (v) BA: both OH bonds pointing away from the graphene sheet (Figure 2g), and (vi) BP: both OH bonds oriented parallel to the graphene sheet (Figure 2h).

For the negatively charged graphene sheet (Figure 2j), $\mathcal{P}(\cos\theta_{\mathrm{DW}}, \cos\theta_{\mathrm{HH}})$ is denser for $\cos\theta_{\mathrm{DW}} < 0$, indicating that most water molecules in the L1 layer adopt VT, BT, and VE configurations. As the graphene sheet becomes neutral (Figure 2k), the distribution shifts to the right, with high density in the VA configuration and the region between BT and BP configurations, with some molecules contributing to VT and VE configurations. When the graphene sheet is positively charged (Figure 2l), nearly all molecules adopt VA, BA and BP configurations, leaving no configurations with $\cos\theta_{\mathrm{DW}} < 0$. This variation of $\mathcal{P}(\cos\theta_{\mathrm{DW}}, \cos\theta_{\mathrm{HH}})$ demonstrates that water molecules orient their OH bonds toward a negatively charged graphene sheet and reorient them away as the graphene sheet becomes positively charged. Additional analyses are reported in the Supporting Information. Specifically, the difference in $\mathcal{P}(\cos\theta_{\mathrm{DW}}, \cos\theta_{\mathrm{HH}})$ distributions between neutral and charged graphene sheets is shown in Figure S2, while Figure S3 shows the molecular orientation distribution as a function of q for five water layers.

HD-vSFG spectrum of the graphene/water interface. To establish a direct link between molecular orientations and structural arrangements identified in the MD simulations and experimentally measurable quantities, we calculated the HD-vSFG spectrum of the graphene/water interface at 298 K using Te-PIGS simulations, which effectively account for NQEs and, therefore, enable realistic comparisons between the experimental and simulated spectra. Analogous HD-vSFG spectra calculated from classical MD simulations are reported in the Supporting Information. Figure 3 shows the imaginary component of the HD-vSFG spectra calculated from Te-PIGS simulations of the graphene/water interface for graphene sheets with varying positive and negative q values. The HD-vSFG spectra were

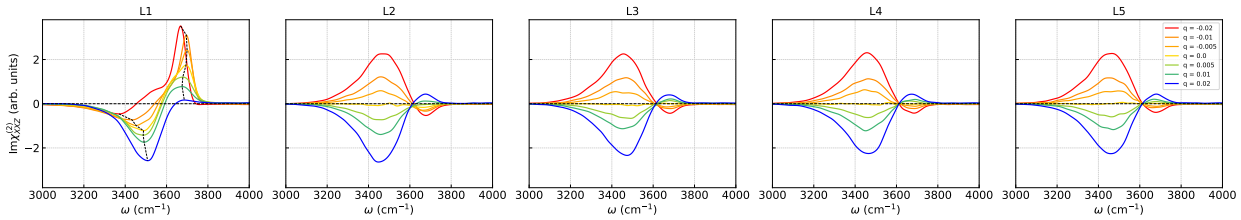

Figure 3: HD-vSFG spectra of the graphene/water interface at 298 K calculated for the SSP polarization combination using Te-PIGS simulations at varying graphene charge values. The spectra are shown for five water layers: L1, L2, L3, L4, and L5. Dashed black lines in L1 track the positions of the negative and positive peaks as the graphene charge varies.

calculated for the SSP polarization combination, where S and P denote laser polarizations parallel and perpendicular to the interface, respectively, using the autocorrelation function scheme discussed in Ref. 6 (see Supporting Information for details). The effects of dipole moment and polarizability cross-correlation terms are investigated in Figures S7 and S8 of the Supporting Information. For neutral graphene sheets, the Te-PIGS HD-vSFG spectrum calculated for water molecules in the L1 layer (Figure 1) reveals two prominent peaks in the OH stretching region: a sharp peak at 3700 cm^{-1} corresponding to the dangling OH bonds and a broad band at 3450 cm^{-1} associated with hydrogen-bonded OH bonds. As q becomes more negative, the water OH bonds orient toward the graphene sheet, increasing the intensity of the dangling OH peak while decreasing the intensity of the hydrogen-bonded OH peak. Conversely, when the graphene sheet is made more positively charged, the intensity of the dangling OH peak decreases, and the intensity of the hydrogen-bonded OH peak increases. Notably, the frequency of the dangling OH peak in the neutral graphene/water interface is found to be red-shifted by 20 cm^{-1} compared to the free OH peak observed at the air/water interface, indicating that the graphene sheet interacts with the free OH group, weakening its bond strength in a manner similar to that reported in Ref. 29. Te-PIGS simulations of the HD-vSFG spectra of the graphene/water interface predict that the dangling OH peak exhibits slightly higher intensity and a broader width compared to the analogous peak at the air/water interface, consistent with previous findings in Ref. 58 (see Figure S8 in the Supporting Information). Interestingly, the position of the dangling OH peak in the

HD-vSFG spectra calculated for varying q values follows a trend similar to the G-band in the Raman spectra of graphene observed experimentally, as the graphene surface charge varies from negative to positive.[9,59] Importantly, the Te-PIGS simulations also show that accurately accounting for NQEs results in a red shift of approximately 150 cm^{-1} in the HD-vSFG spectrum of the graphene/water interface relative to the corresponding spectrum calculated from classical MD simulations (see Figure S6 in the Supporting Information). This shift is slightly smaller than the 175 cm^{-1} red shift calculated for the analogous HD-vSFG spectrum of the air/water interface calculated from classical MD and centroid molecular dynamics (CMD) simulations with MB-pol.[5,6]

The impact of graphene surface charge on the contributions to the HD-vSFG spectra from deeper water layers is particularly intriguing. For a neutral graphene sheet ($q = 0.0e$), the spectral contribution from water layers beyond L2 is negligible, as expected for a centrosymmetric bulk medium. However, in the presence of charged graphene sheets, contributions to the HD-vSFG spectra from these deeper layers become significant. As the graphene sheet becomes negatively charged, the intensity of the hydrogen-bonded band becomes more positive, while the peak at 3700 cm^{-1} becomes more negative. Conversely, for the positively charged graphene sheet, the hydrogen-bonded band becomes more negative, and the peak at 3700 cm^{-1} becomes more positive. These changes in the contributions to the HD-vSFG spectra from different water layers arise as the OH bonds of hydrogen-bonded molecules increasingly align toward the negatively charged graphene sheet. This is further illustrated in Figure S4, where the HD-vSFG spectrum calculated for $q = -0.02e$ displays a positive peak in the hydrogen-bonded region that increases with depth. A similar trend has been observed in MD simulations of electrode/aqueous electrolyte interfaces.[10]

Given the significance of bulk contributions in shaping the vSFG response, it becomes essential to quantify the role of the bulk third-order susceptibility, $\chi^{(3)}$, which accounts for the influence of the interfacial electric field on the deeper water layers. Unlike the second-order susceptibility, $\chi^{(2)}$, which is sensitive to water molecules near the interface where inversion

symmetry is broken, the third-order susceptibility, $\chi^{(3)}$, arises from regions within the bulk allowing water molecules farther from the interface to contribute to the vSFG signal. This is particularly relevant near charged or highly polarizable interfaces, where the electric field penetrates into the bulk, aligning water dipoles and creating a structured response that can subtly alter the corresponding vSFG spectra.[41] However, as illustrated in Figure S5 of the Supporting Information, the $\chi^{(3)}$ contribution to the HD-vSFG spectra of both neutral and charged graphene/water interfaces appears around 3200 cm^{-1} and is an order of magnitude smaller than the $\chi^{(2)}$ contribution, resulting in minimal effects on the HD-vSFG spectra. This indicates that, while $\chi^{(3)}$ contributions are present, their impact on the overall HD-vSFG response is negligible in comparison to the dominant $\chi^{(2)}$ contributions.

Spectral decomposition. To pinpoint the origins of the various spectral features, we decomposed the HD-vSFG spectra from the L1 and L2 layers according to molecular orientations and hydrogen-bonding topologies. In the analysis of molecular orientations, all water molecules were grouped into four categories: (i) BA, (ii) VA, (iii) BT, and (iv) VT, resembling the definitions introduced in Figure 2. BP and VE configurations defined in Figure 2 are ignored as they do not contribute to the HD-vSFG spectra in the SSP polarization combination considered in this study. In the case of water molecules in the L1 layer in contact with a neutral graphene sheet, Figure 4 shows that BA molecules contribute to a negative hydrogen-bonded OH band at 3500 cm^{-1}, VA molecules contribute to both a negative peak at 3450 cm^{-1} and a positive peak at 3700 cm^{-1}, BT molecules contribute to a positive peak at 3500 cm^{-1}, and VT molecules contribute to both a positive peak at 3700 cm^{-1} and a negative peak at 3450 cm^{-1}. As the graphene becomes more negatively charged, the intensity of the peak due to BA molecules decreases, while the intensities of the peaks due to BT and VT molecules increase.

For neutral graphene sheets, the analysis of the contributions to the HD-vSFG spectra from water molecules in the L2 layer reveals that most spectral features resemble those of

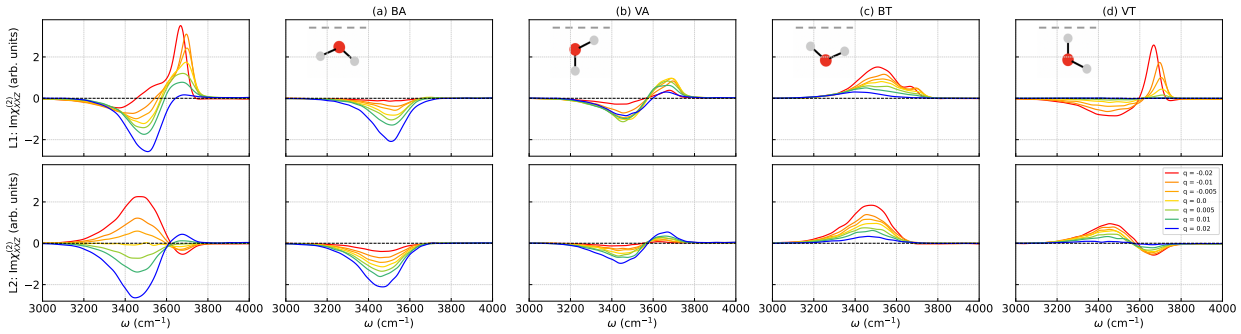

Figure 4: Spectral decomposition of the Te-PIGS HD-vSFG spectra of the graphene/water interface at 298 K for varying graphene surface charges calculated for the SSP polarization combination considering water molecules in the L1 (top row) and L2 (bottom row) layers. In this analysis, water molecules are classified according to their molecular orientations: (a) BA: both OH bonds pointing away from the surface, (b) VA: vertical OH bond pointing away from the surface, (c) BT: both OH bonds pointing toward the surface, and (d) VT: vertical OH bond pointing toward the surface.

molecules in the L1 layer. There are, however, some differences. Notably, VT molecules in the L2 layer are responsible for a positive peak at 3450 cm^{-1} and a negative peak at 3700 cm^{-1}, opposite to what is observed for VT molecules in the L1 layer. This can be understood by considering that vertical OH bonds of VT molecules in the L1 layer are stronger because they are dangling OH bonds not involved in hydrogen bonding. However, for molecules in the L2 layer, these vertical OH bonds engage in hydrogen bonding, causing them to weaken and shift to lower frequencies. In contrast, the non-vertical OH bonds of VT molecules in the L1 layer are initially weaker, as electron density is drawn toward the vertical OH bonds. This electron migration results in the non-vertical OH bonds in the L2 layer gaining electron density, which, in turn, cause them to strengthen and shift to higher frequencies. Importantly, for a neutral graphene sheet, the contributions from BA and BT molecules within the L2 layer cancel each other, as do the contributions from VA and VT molecules. However, for charged graphene sheets, because of unequal populations of molecules pointing their OH bonds toward and away from the graphene sheet, the contributions from BA and BT molecules in the L2 layer do not fully cancel, resulting in an intense positive (negative) peak in the hydrogen-bonded region in the case of a negatively (positively) charged graphene

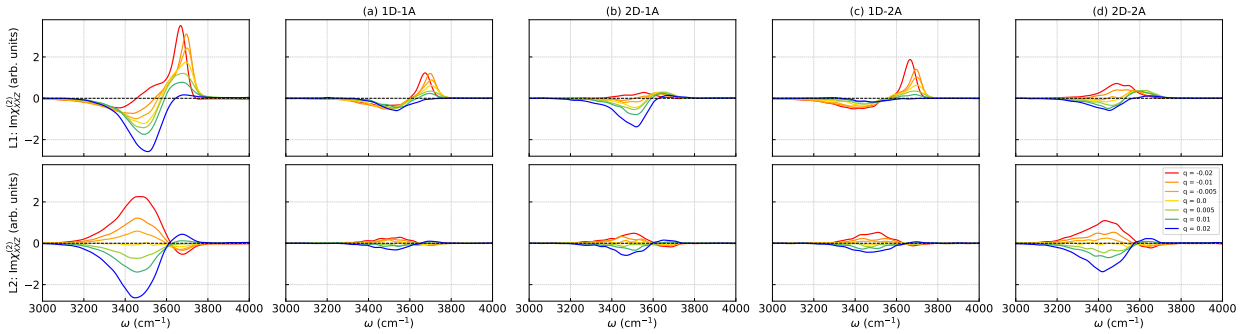

Figure 5: Spectral decomposition of the Te-PIGS vSFG spectrum at 298 K for varying graphene surface charges. The analysis categorizes water molecules by hydrogen bonding topologies, (a) 1D-1A, (b) 2D-1A, (c) 1D-2A, and (d) 2D-2A in L1 (upper row) and L2 layers (lower row). All vSFG spectra were calculated for the SSP polarization combination.

sheet. Moreover, for charged graphene sheets, the contributions from VA and VT molecules in the L2 layer also do not fully compensate resulting in a high-frequency positive (negative) peak in the case of a positively (negatively) charged graphene sheet.

Additional insights into the structure of water at the interface with neutral and charged graphene sheets are gained from analyzing the underlying hydrogen-bonding topologies. Figure 5 illustrates the decomposition of the HD-vSFG spectra into contributions from single donor-single acceptor (1D-1A) molecules (a), double donor-single acceptor (2D-1A) molecules (b), single donor-double acceptor (1D-2A) molecules (c), and double donor-double acceptor (2D-2A) molecules (d) in the L1 and L2 layers. In the L1 layer, VT and BA molecules exhibit 1D-2A and 2D-1A hydrogen-bonding topologies, respectively, whereas in the L2 layer, most molecules adopt a 2D-2A hydrogen-bonding topology. The similarity between the spectral decompositions from quantum Te-PIGS simulations (Figures 4 and 5) and from classical MD simulations (Figure S9 and Figure S10) demonstrates that NQEs do not affect the structure and hydrogen-bonding topolgies of water molecules at the interface of both neutral and charged graphene sheets.

Comparisons with experimental results indicate that the Te-PIGS HD-vSFG spectra for water in the L1 layer are consistent with recent measurements on neutral substrate-free graphene,[29] showing a positive dangling OH peak. A direct comparison with the experi-

mental spectra reported in Ref. 9 is not possible, as those experiments were performed on a graphene sheet supported on CaF_2 substrate. Nevertheless, the Te-PIGS HD-vSFG spectra follow the same frequency shift and peak intensity trends observed in the experiments conducted for both positively and negatively charged graphene sheets. Moreover, the Te-PIGS HD-vSFG spectra calculated for water molecules in the L1 and L2 layers, as the graphene charge varies from positive to negative, are consistent with the experimental decomposition into surface and bulk contributions.

Conclusions

In this study, we combined the MB-pol data-driven many-body potential with path-integral-based quantum simulations to investigate the structure and vibrational response of water at neutral and charged graphene interfaces, revealing how varying surface charges influence the orientation and hydrogen-bonding topologies of interfacial water molecules.

For neutral graphene, water molecules primarily adopt configurations with a vertical OH bond pointing away from the interface. As the surface charge becomes increasingly negative, configurations with vertical OH bonds pointing toward the interface become dominant. Conversely, positive charges on graphene promote configurations where water molecules orient a vertical OH bond away from the interface. These charge-induced structural rearrangements result in specific spectral features associated with molecules in the first interfacial layer, including a pronounced dangling OH peak from molecules with vertical OH bonds pointing toward negatively charged graphene and a broader hydrogen-bonded band from molecules with one or both OH bonds oriented away from the graphene sheet. These structural motifs extend into deeper water layers, creating an imbalance in the population of molecules with OH bonds pointing toward and away from the graphene sheets suggesting that charged graphene sheets can modulate the properties of water even in subsurface layers.

Comparisons with recent measurements show that the simulations capture all trends

observed in the experimental HD-vSFG spectra, including intensity variations in the dangling OH peak and hydrogen-bonded OH band, as well as electric-field-induced vibrational frequency shifts. The agreement between experimental and simulated HD-vSFG spectra provides strong evidence for the realism of the MB-pol potential, highlighting the importance of accurately representing many-body interactions and incorporating nuclear quantum effects to model vibrational spectra of water across different environments. Future work will explore the effects of graphene polarizability[60] and dynamic flow conditions[26] to refine the molecular understanding of neutral and charged graphene/water interfaces, offering further insights for designing advanced materials for applications ranging from energy storage to catalysis and filtration.

Methods

Molecular dynamics simulations. The initial configuration of graphene/water interface was prepared using MakeGraphitics library[61] and PACKMOL.[62] All simulations were carried out in periodic boundary conditions for a water slab containing $N = 512$ water molecules with two graphene sheets on either side each with 180 carbon atoms. The graphene sheet was modeled using the three-body Tersoff potential[63,64] and the non-bonded interactions between MB-pol water and the graphene carbon were described by a Lennard-Jones potential, whose parameters were optimized using the Lorentz-Berthelot mixing rule. The classical vSFG spectra were calculated from classical MD simulations in the NVE ensemble performed using MBX[65] combined with LAMMPS.[66] The quantum vSFG spectra were calculated from Te-PIGS simulations performed using MBX[65] combined with DeePMD[67] and i-PI[68] with MB-pol + QC@MB-pol (quantum correction potential) in the NVE ensemble. Specific details about the training and validation of the quantum correction QC@MB-pol potential and Te-PIGS simulations are discussed in the Supporting Information.

vSFG spectrum calculations. The many-body dipole moment surface (MB-μ) and polarizability surface (MB-α) were used to compute the dipole moments and polarizability tensors.[69] The second-order susceptibility $\chi^{(2)}_{ijk}(\omega)$ was calculated from the Fourier transform of the time correlation function (TCF) of the dipole moment and polarizability tensor.[70,71] The total time correlation function was computed as a sum of the autocorrelation function and truncated cross-correlation function over all water molecules within a cutoff distance of 4.0 Å.[5,6] The bulk $\chi^{(3)}$ contribution was computed with a $\chi^{(2)}/\chi^{(3)}$ scaling factor of 120 using the methods mentioned in 72–74. Further details of the vSFG spectra and spectral decomposition calculations are discussed in the Supporting Information.

Acknowledgement

This research was supported by the National Science Foundation through grant no. 2311260. Computational resources were provided by the Advanced Cyberinfrastructure Coordination Ecosystem: Services & Support (ACCESS) program, which is supported by National Science Foundation grants nos. 2138259, 2138286, 2138307, 2137603, and 2138296, the Triton Shared Computing Cluster (TSCC) at the San Diego Supercomputer Center (SDSC) at UC San Diego, and the LSU-HPC and LONI HPC facilities at Lousiana Sate University.

Supporting Information Available

Details about initial configurations, potential energy surfaces, equilibration and production simulations, HD-vSFG spectrum calculations, spectral decompositions, tetrahedral order parameter calculations, and dielectric constant calculations.

References

1. Eisenberg, D.; Kauzmann, W. *The Structure and Properties of Water*; Clarendon Press, 1969.

2. Maréchal, Y. *The Hydrogen Bond and the Water Molecule: The Physics and Chemistry of Water, Aqueous and Bio-media*; Elsevier, 2006.

3. Björneholm, O.; Hansen, M. H.; Hodgson, A.; Liu, L.-M.; Limmer, D. T.; Michaelides, A.; Pedevilla, P.; Rossmeisl, J.; Shen, H.; Tocci, G.; Tyrode, E.; Walz, M. M.; Werner, J.; Bluhm, H. Water at Interfaces. *Chem. Rev.* **2016**, *116*, 7698–7726.

4. Stiopkin, I. V.; Weeraman, C.; Pieniazek, P. A.; Shalhout, F. Y.; Skinner, J. L.; Benderskii, A. V. Hydrogen Bonding at the Water Surface Revealed by Isotopic Dilution Spectroscopy. *Nature* **2011**, *474*, 192–195.

5. Medders, G. R.; Paesani, F. Dissecting the Molecular Structure of the Air/Water Interface from Quantum Simulations of the Sum-Frequency Generation Spectrum. *J. Am. Chem. Soc.* **2016**, *138*, 3912–3919.

6. Moberg, D. R.; Straight, S. C.; Paesani, F. Temperature Dependence of the Air/Water Interface Revealed by Polarization Sensitive Sum-Frequency Generation Spectroscopy. *J. Phys. Chem. B* **2018**, *122*, 4356–4365.

7. Rajamani, S.; Ghosh, T.; Garde, S. Size Dependent Ion Hydration, Its Asymmetry, and Convergence to Macroscopic Behavior. *J. Chem. Phys.* **2004**, *120*, 4457–4466.

8. Gonella, G.; Backus, E. H.; Nagata, Y.; Bonthuis, D. J.; Loche, P.; Schlaich, A.; Netz, R. R.; Kühnle, A.; McCrum, I. T.; Koper, M. T.; Wolf, M.; Winter, B.; Meijer, G.; Campen, R. K.; Bonn, M. Water at Charged Interfaces. *Nat. Rev. Chem.* **2021**, *5*, 466–485.

9. Montenegro, A.; Dutta, C.; Mammetkuliev, M.; Shi, H.; Hou, B.; Bhattacharyya, D.; Zhao, B.; Cronin, S. B.; Benderskii, A. V. Asymmetric Response of Interfacial Water to Applied Electric Fields. *Nature* **2021**, *594*, 62–65.

10. Olivieri, J.-F.; Hynes, J. T.; Laage, D. Water Dynamics and Sum-Frequency Generation Spectra at Electrode/Aqueous Electrolyte Interfaces. *Faraday Discuss.* **2024**, *249*, 289–302.

11. Geim, A. K.; Novoselov, K. S. The Rise of Graphene. *Nat. Mater.* **2007**, *6*, 183–191.

12. Novoselov, K. S.; Geim, A. K.; Morozov, S. V.; Jiang, D.-e.; Zhang, Y.; Dubonos, S. V.; Grigorieva, I. V.; Firsov, A. A. Electric Field Effect in Atomically Thin Carbon Films. *Science* **2004**, *306*, 666–669.

13. Novoselov, K. S.; Geim, A. K.; Morozov, S. V.; Jiang, D.; Katsnelson, M. I.; Grigorieva, I. V.; Dubonos, S. V.; Firsov, A. A. Two-Dimensional Gas of Massless Dirac Fermions in Graphene. *Nature* **2005**, *438*, 197–200.

14. Balandin, A. A.; Ghosh, S.; Bao, W.; Calizo, I.; Teweldebrhan, D.; Miao, F.; Lau, C. N. Superior Thermal Conductivity of Single-Layer Graphene. *Nano Lett.* **2008**, *8*, 902–907.

15. Liu, G.; Jin, W.; Xu, N. Graphene-Based Membranes. *Chem. Soc. Rev.* **2015**, *44*, 5016–5030.

16. Wu, D.; Zhao, Z.; Lin, B.; Song, Y.; Qi, J.; Jiang, J.; Yuan, Z.; Cheng, B.; Zhao, M.; Tian, Y.; Wang, Z.; Wu, M.; Bian, K.; Liu, K.-H.; Xu, L.-M.; Zeng, X. C.; Wang, E.-G.; Jiang, Y. Probing Structural Superlubricity of Two-Dimensional Water Transport with Atomic Resolution. *Science* **2024**, *384*, 1254–1259.

17. Taherian, F.; Marcon, V.; van der Vegt, N. F.; Leroy, F. What Is the Contact Angle of Water on Graphene? *Langmuir* **2013**, *29*, 1457–1465.

18. Prydatko, A. V.; Belyaeva, L. A.; Jiang, L.; Lima, L. M.; Schneider, G. F. Contact Angle Measurement of Free-Standing Square-Millimeter Single-Layer Graphene. *Nat. Commun.* **2018**, *9*, 4185.

19. Carlson, S. R.; Schullian, O.; Becker, M. R.; Netz, R. R. Modeling Water Interactions with Graphene and Graphite via Force Fields Consistent with Experimental Contact Angles. *J. Phys. Chem. Lett.* **2024**, *15*, 6325–6333.

20. Shen, Y. Phase-Sensitive Sum-Frequency Spectroscopy. *Annu. Rev. Phys. Chem.* **2013**, *64*, 129–150.

21. Singla, S.; Anim-Danso, E.; Islam, A. E.; Ngo, Y.; Kim, S. S.; Naik, R. R.; Dhinojwala, A. Insight on Structure of Water and Ice Next to Graphene Using Surface-Sensitive Spectroscopy. *ACS Nano* **2017**, *11*, 4899–4906.

22. Dreier, L. B.; Liu, Z.; Narita, A.; Van Zadel, M.-J.; Müllen, K.; Tielrooij, K.-J.; Backus, E. H.; Bonn, M. Surface-Specific Spectroscopy of Water at a Potentiostatically Controlled Supported Graphene Monolayer. *J. Phys. Chem. C* **2019**, *123*, 24031–24038.

23. Tsai, M.-H.; Lu, Y.-X.; Lin, C.-Y.; Lin, C.-H.; Wang, C.-C.; Chu, C.-M.; Woon, W.-Y.; Lin, C.-T. The First-Water-Layer Evolution at the Graphene/Water Interface Under Different Electro-Modulated Hydrophilic Conditions Observed by Suspended/Supported Field-Effect-Device Architectures. *ACS Appl. Mater. Interfaces* **2023**, *15*, 17019–17028.

24. Kim, D.; Kim, E.; Park, S.; Kim, S.; Min, B. K.; Yoon, H. J.; Kwak, K.; Cho, M. Wettability of Graphene and Interfacial Water Structure. *Chem* **2021**, *7*, 1602–1614.

25. Yang, S.; Zhao, X.; Lu, Y.-H.; Barnard, E. S.; Yang, P.; Baskin, A.; Lawson, J. W.; Prendergast, D.; Salmeron, M. Nature of the Electrical Double Layer on Suspended Graphene Electrodes. *J. Am. Chem. Soc.* **2022**, *144*, 13327–13333.

26. Wang, Y.; Seki, T.; Yu, X.; Yu, C.-C.; Chiang, K.-Y.; Domke, K. F.; Hunger, J.; Chen, Y.; Nagata, Y.; Bonn, M. Chemistry Governs Water Organization at a Graphene Electrode. *Nature* **2023**, *615*, E1–E2.

27. Wang, Y.; Seki, T.; Liu, X.; Yu, X.; Yu, C.-C.; Domke, K. F.; Hunger, J.; Koper, M. T.; Chen, Y.; Nagata, Y.; Bonn, M. Direct Probe of Electrochemical Pseudocapacitive pH Jump at a Graphene Electrode. *Angew. Chem. Int. Ed.* **2023**, *62*, e202216604.

28. Wang, Y.; Nagata, Y.; Bonn, M. Substrate Effect on Charging of Electrified Graphene/Water Interfaces. *Faraday Discuss.* **2024**, *249*, 303–316.

29. Wang, Y.; Tang, F.; Yu, X.; Ohto, T.; Nagata, Y.; Bonn, M. Heterodyne-Detected Sum-Frequency Generation Vibrational Spectroscopy Reveals Aqueous Molecular Structure at the Suspended Graphene/Water Interface. *Angew. Chem. Int. Ed.* **2024**, *63*, e202319503.

30. Rana, M. K.; Chandra, A. Ab Initio and Classical Molecular Dynamics Studies of the Structural and Dynamical Behavior of Water Near a Hydrophobic Graphene Sheet. *J. Chem. Phys.* **2013**, *138*, 204702.

31. Ohto, T.; Tada, H.; Nagata, Y. Structure and Dynamics of Water at Water-Graphene and Water-Hexagonal Boron-Nitride Sheet Interfaces Revealed by Ab Initio Sum-Frequency Generation Spectroscopy. *Phys. Chem. Chem. Phys.* **2018**, *20*, 12979–12985.

32. Gillan, M. J.; Alfe, D.; Michaelides, A. Perspective: How Good is DFT for Water? *J. Chem. Phys.* **2016**, *144*, 130901.

33. Dasgupta, S.; Lambros, E.; Perdew, J. P.; Paesani, F. Elevating Density Functional Theory to Chemical Accuracy for Water Simulations Through a Density-Corrected Many-Body Formalism. *Nat. Commun.* **2021**, *12*, 1–12.

34. Palos, E.; Lambros, E.; Swee, S.; Hu, J.; Dasgupta, S.; Paesani, F. Assessing the Inter-

play Between Functional-Driven and Density-Driven Errors in DFT Models of Water. *J. Chem. Theory Comput.* **2022**, *18*, 3410–3426.

35. Cisneros, G. A.; Wikfeldt, K. T.; Ojamäe, L.; Lu, J.; Xu, Y.; Torabifard, H.; Bartók, A. P.; Csányi, G.; Molinero, V.; Paesani, F. Modeling Molecular Interactions in Water: From Pairwise to Many-Body Potential Energy Functions. *Chem. Rev.* **2016**, *116*, 7501–7528.

36. Riera, M.; Lambros, E.; Nguyen, T. T.; Götz, A. W.; Paesani, F. Low-Order Many-Body Interactions Determine the Local Structure of Liquid Water. *Chem. Sci.* **2019**, *10*, 8211–8218.

37. Bore, S. L.; Paesani, F. Realistic Phase Diagram of Water from "First Principles" Data-Driven Quantum Simulations. *Nat. Commun.* **2023**, *14*, 3349.

38. Montero de Hijes, P.; Dellago, C.; Jinnouchi, R.; Kresse, G. Density Isobar of Water and Melting Temperature of Ice: Assessing Common Density Functionals. *J. Chem. Phys.* **2024**, *161*, 131102.

39. Howard, J. C.; Enyard, J. D.; Tschumper, G. S. Assessing the Accuracy of Some Popular DFT Methods for Computing Harmonic Vibrational Frequencies of Water Clusters. *J. Chem. Phys.* **2015**, *143*, 214103.

40. Marsalek, O.; Markland, T. E. Quantum Dynamics and Spectroscopy of Ab Initio Liquid Water: The Interplay of Nuclear and Electronic Quantum Effects. *J. Phys. Chem. Lett.* **2017**, *8*, 1545–1551.

41. Joutsuka, T.; Hirano, T.; Sprik, M.; Morita, A. Effects of Third-Order Susceptibility in Sum Frequency Generation Spectra: A Molecular Dynamics Study in Liquid Water. *Phys. Chem. Chem. Phys.* **2018**, *20*, 3040–3053.

42. Zhang, Y.; de Aguiar, H. B.; Hynes, J. T.; Laage, D. Water Structure, Dynamics, and Sum-Frequency Generation Spectra at Electrified Graphene Interfaces. *J. Phys. Chem. Lett.* **2020**, *11*, 624–631.

43. Zhang, Y.; Stirnemann, G.; Hynes, J. T.; Laage, D. Water Dynamics at Electrified Graphene Interfaces: A Jump Model Perspective. *Phys. Chem. Chem. Phys.* **2020**, *22*, 10581–10591.

44. Vega, C.; Abascal, J. L. Simulating Water with Rigid Non-Polarizable Models: A General Perspective. *Phys. Chem. Chem. Phys.* **2011**, *13*, 19663–19688.

45. Medders, G. R.; Paesani, F. On the Interplay of the Potential Energy and Dipole Moment Surfaces in Controlling the Infrared Activity of Liquid Water. *J. Chem. Phys.* **2015**, *142*, 212411.

46. Babin, V.; Leforestier, C.; Paesani, F. Development of a "First Principles" Water Potential with Flexible Monomers: Dimer Potential Energy Surface, VRT Spectrum, and Second Virial Coefficient. *J. Chem. Theory Comput.* **2013**, *9*, 5395–5403.

47. Babin, V.; Medders, G. R.; Paesani, F. Development of a "First Principles" Water Potential with Flexible monomers. II: Trimer Potential Energy Surface, Third Virial Coefficient, and Small Clusters. *J. Chem. Theory Comput.* **2014**, *10*, 1599–1607.

48. Medders, G. R.; Babin, V.; Paesani, F. Development of a "First-Principles" Water Potential with Flexible Monomers. III. Liquid Phase Properties. *J. Chem. Theory Comput.* **2014**, *10*, 2906–2910.

49. Zhu, X.; Riera, M.; Bull-Vulpe, E. F.; Paesani, F. MB-pol(2023): Sub-chemical Accuracy for Water Simulations from the Gas to the Liquid Phase. *J. Chem. Theory Comput.* **2023**, *19*, 3551–3566.

50. Reddy, S. K.; Straight, S. C.; Bajaj, P.; Huy Pham, C.; Riera, M.; Moberg, D. R.; Morales, M. A.; Knight, C.; Götz, A. W.; Paesani, F. On the Accuracy of the MB-pol Many-Body Potential for Water: Interaction Energies, Vibrational Frequencies, and Classical Thermodynamic and Dynamical Properties from Clusters to Liquid water and Ice. *J. Chem. Phys.* **2016**, *145*, 194504.

51. Palos, E.; Bull-Vulpe, E. F.; Zhu, X.; Agnew, H.; Gupta, S.; Paesani, F. Current Status of the MB-pol Data-Driven Many-Body Potential for Predictive Simulations of Water Across Different Phases. *J. Chem. Theory Comput.* **2024**, *20*, 9269–9289.

52. Musil, F.; Zaporozhets, I.; Noé, F.; Clementi, C.; Kapil, V. Quantum Dynamics Using Path Integral Coarse-graining. *J. Chem. Phys.* **2022**, *157*, 181102.

53. Kapil, V.; Kovács, D. P.; Csányi, G.; Michaelides, A. First-principles Spectroscopy of Aqueous Interfaces using Machine-learned Electronic and Quantum Nuclear Effects. *Faraday Discuss.* **2024**, *249*, 50–68.

54. Subasinghege Don, V.; David, R.; Du, P.; Milet, A.; Kumar, R. Interfacial Water at Graphene Oxide Surface: Ordered or Disordered? *J. Phys. Chem. B* **2019**, *123*, 1636–1649.

55. David, R.; Tuladhar, A.; Zhang, L.; Arges, C.; Kumar, R. Effect of Oxidation Level on the Interfacial Water at the Graphene Oxide–Water Interface: From Spectroscopic Signatures to Hydrogen-Bonding Environment. *J. Phys. Chem. B* **2020**, *124*, 8167–8178.

56. Subasinghege Don, V.; Kim, L.; David, R.; Nauman, J. A.; Kumar, R. Adsorption Studies at the Graphene Oxide–Liquid Interface: A Molecular Dynamics Study. *J. Phys. Chem. C* **2023**, *127*, 5920–5930.

57. Azom, G.; Milet, A.; David, R.; Kumar, R. From Graphene Oxide to Graphene: Changes in Interfacial Water Structure and Reactivity Using Deep Neural Network Force Fields. *J. Phys. Chem. C* **2024**, *128*, 16437.

58. Xu, Y.; Ma, Y.-B.; Gu, F.; Yang, S.-S.; Tian, C.-S. Structure Evolution at the Gate-Tunable Suspended Graphene–Water Interface. *Nature* **2023**, *621*, 506–510.

59. Wang, Y.; Seki, T.; Gkoupidenis, P.; Chen, Y.; Nagata, Y.; Bonn, M. Aqueous Chemimemristor Based on Proton-Permeable Graphene Membranes. *Proc. Natl. Acad. Sci. U.S.A.* **2024**, *121*, e2314347121.

60. Ho, T. A.; Striolo, A. Polarizability Effects in Molecular Dynamics Simulations of the Graphene–Water Interface. *J. Chem. Phys.* **2013**, *138*, 054117.

61. Sinclair, R. C.; Coveney, P. V. Modelling Nanostructure in Graphene Oxide: Inhomogeneity and the Percolation Threshold. *J. Chem. Inf. Model.* **2019**, *59*, 2741–2745.

62. Martínez, L.; Andrade, R.; Birgin, E. G.; Martínez, J. M. PACKMOL: A Package for Building Initial Configurations for Molecular Dynamics Simulations. *J. Comput. Chem.* **2009**, *30*, 2157–2164.

63. Tersoff, J. Empirical Interatomic Potential for Silicon with Improved Elastic Properties. *Phys. Rev. B* **1988**, *38*, 9902.

64. Tersoff, J. Modeling Solid-State Chemistry: Interatomic Potentials for Multicomponent Systems. *Phys. Rev. B* **1989**, *39*, 5566.

65. Riera, M.; Knight, C.; Bull-Vulpe, E. F.; Zhu, X.; Agnew, H.; Smith, D. G. A.; Simmonett, A. C.; Paesani, F. MBX: A Many-Body Energy and Force Calculator for Data-Driven Many-Body Simulations. *J. Chem. Phys.* **2023**, *159*, 054802.

66. Thompson, A. P.; Aktulga, H. M.; Berger, R.; Bolintineanu, D. S.; Brown, W. M.; Crozier, P. S.; in 't Veld, P. J.; Kohlmeyer, A.; Moore, S. G.; Nguyen, T. D.; Shan, R.; Stevens, M. J.; Tranchida, J.; Trott, C.; Plimpton, S. J. LAMMPS – A Flexible Simulation Tool for Particle-Based Materials Modeling at the Atomic, Meso, and Continuum Scales. *Comput. Phys. Commun.* **2022**, *271*, 108171.

67. Wang, H.; Zhang, L.; Han, J.; Weinan, E. DeePMD-kit: A Deep Learning Package for Many-Body Potential Energy Representation and Molecular Dynamics. *Comput. Phys. Commun.* **2018**, *228*, 178–184.

68. Kapil, V.; Rossi, M.; Marsalek, O.; Petraglia, R.; Litman, Y.; Spura, T.; Cheng, B.; Cuzzocrea, A.; Meißner, R. H.; Wilkins, D. M.; Juda, P.; Bienvenue, S. P.; Fang, W.; Kessler, J.; Poltavsky, I.; Vandenbrande, S.; Wieme, J.; Corminboeuf, C.; Kühne, T. D.; Manolopoulos, D. E.; Markland, T. E.; Richardson, J. O.; Tkatchenko, A.; Tribello, G. A.; Van Speybroeck, V.; Ceriotti, M. i-PI 2.0: A Universal Force Engine for Advanced Molecular Simulations. *Comput. Phys. Commun.* **2019**, *236*, 214–223.

69. Medders, G. R.; Paesani, F. Infrared and Raman Spectroscopy of Liquid Water through "First-Principles" Many-Body Molecular Dynamics. *J. Chem. Theory Comput.* **2015**, *11*, 1145–1154.

70. Morita, A.; Hynes, J. T. A Theoretical Analysis of the Sum Frequency Generation Spectrum of the Water Surface. II. Time-Dependent Approach. *J. Phys. Chem. B* **2002**, *106*, 673–685.

71. Nagata, Y.; Mukamel, S. Vibrational Sum-Frequency Generation Spectroscopy at the Water/Lipid Interface: Molecular Dynamics Simulation Study. *J. Am. Chem. Soc.* **2010**, *132*, 6434–6442.

72. Ohno, P. E.; Wang, H.-f.; Paesani, F.; Skinner, J. L.; Geiger, F. M. Second-Order Vibrational Lineshapes from the Air/Water Interface. *J. Phys. Chem. A* **2018**, *122*, 4457–4464.

73. Reddy, S. K.; Thiraux, R.; Rudd, B. A. W.; Lin, L.; Adel, T.; Joutsuka, T.; Geiger, F. M.; Allen, H. C.; Morita, A.; Paesani, F. Bulk Contributions Modulate the Sum-Frequency Generation Spectra of Water on Model Sea-Spray Aerosols. *Chem* **2018**, *4*, 1629–1644.

74. Moberg, D. R.; Li, Q.; Reddy, S. K.; Paesani, F. Water Structure at the Interface of Alcohol Monolayers as Determined by Molecular Dynamics Simulations and Computa-

tional Vibrational Sum-Frequency Generation Spectroscopy. *J. Chem. Phys.* **2019**, *150*, 034701.

TOC Graphic